JACS
JOURNAL OF THE AMERICAN CHEMICAL SOCIETY
Article
pubs.acs.org/JACS

Magnetocurrent of Charge-Polarizable C_{60}-Diphenylaminofluorene Monoadduct-Derived Magnetic Nanocomposites

Liang Yan,[†] Min Wang,[‡] N. P. Raju,[§] Arthur Epstein,[§] Loon-Seng Tan,[∥] Augustine Urbas,[∥] Long Y. Chiang,*[,‡] and Bin Hu*[,†]

[†]Department of Materials Science and Engineering, University of Tennessee, Knoxville, Tennessee 37996, United States
[‡]Department of Chemistry, Institute of Nanoscience and Engineering Technology, University of Massachusetts, Lowell, Massachusetts 01854, United States
[§]Department of Physics, Ohio State University, Columbus, Ohio 43210, United States
[∥]AFRL/RXBN, Air Force Research Laboratory, Wright-Patterson Air Force Base, Dayton, Ohio 45433, United States

Supporting Information

ABSTRACT: We demonstrated the strategy of a nanocomposite design by the incorporation of both a delocalized π-electrons system in a closely bound acceptor−donor analogue chromophore, based on charge-polarizable C_{60}(>DPAF-C_9) nanostructure **1**, and spin-polarized d-electrons in the form of γ-FeO_x nanoparticles. Facile intramolecular electron transfer from the DPAF-C_9 donor moiety to the C_{60} acceptor cage of **1** upon activation to the excited state with a long lifetime of the charge-separated state forms a possible mechanism to integrate semiconducting and magnetic properties in a single system. We observed an appreciable magnetocurrent (MC) of C_{60}(>DPAF-C_9)-encapsulated magnetic γ-FeO_x nanoparticles in PMMA matrix upon applying a magnetic field from 0 to 300 mT at either 77 K (12% MC) or 300 K (4.5% MC). Interestingly, the detailed analysis of magnetocurrent curve profiles taken at 77 K allowed us to conclude that the measured magnetocurrent may be attributed to the contributions from magnetic field-dependent excited-state populations in semiconducting structure (density-based MC), magnetism from magnetic structure (mobility-based MC), and product of density and mobility-based MC components (π−d electronic coupling). At the higher temperature region up to 300 K, the semiconducting mechanism dominated the determining factor of measured magnetocurrent. This experimental observation indicated the feasibility of combining delocalized π electrons and spin-polarized d electrons through charge transfer to induce internally coupled dual mobility- and density-based MC through the modulation of spin polarization and excited states in semiconducting/magnetic hybrid materials.

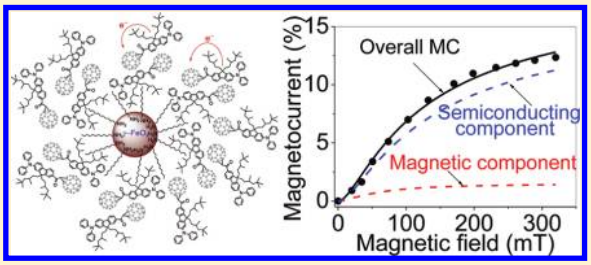

1. INTRODUCTION

The magnetocurrent (MC) phenomena were demonstrated on both organic semiconducting and magnetic materials.[1−9] In general, the MC can be detected as a function of either the spin-dependent charge density or the spin-dependent charge mobility, based on the drift theory: $J = n\mu qE$, where n is the spin-dependent carrier density, μ is the spin-dependent carrier mobility, q is the electron charge, and E is the applied electric field. In the case of charge density-based MC, the spin-population ratio of singlet and triplet excited states may be changed by a magnetic field via perturbation of the singlet−triplet intersystem crossing efficiency based on the spin-momentum conservation. When singlet and triplet excited states generate free charge carriers at a different rate, the related MC can be induced accordingly. In the other case, intercharge spin−spin interactions can be affected by a magnetic field that leads to a mobility-based MC when the spin-scattering is considered during the charge transport. These two arguments clearly require the presence of excited states and intercharge spin−spin interactions in the consideration of the density[10−13]- and mobility[14−18]-based MC, respectively. Experimentally, it was found that organic semiconductors exhibited mainly charge-density-based MC via the facile occurrence of multiple excited states[10,11,19−21] in their π-conjugation systems. However, the same materials usually show negligible mobility-based MC.[22−25] This implied the lack of intercharge spin−spin interactions in organic semiconducting materials under normal operating conditions. On the contrast, these interactions considerably dominate in inorganic magnetic materials that result in the observation of mobility-based magnetocurrent[26,27] as a common phenomenon. It should be noted that inorganic magnetic materials do not possess delocalized π-electrons and, consequently, lack the corresponding excited states. This intrinsic limitation provides the rationale of difficulty in creating density-based MC on this type of materials.

Herein, we report the synthesis and physical property studies of charge-polarizable fullerenyl chromophore C_{60}(>DPAF-C_9)

Received: November 29, 2011
Published: February 10, 2012

dx.doi.org/10.1021/ja210812u | J. Am. Chem. Soc. 2012, 134, 3549−3554

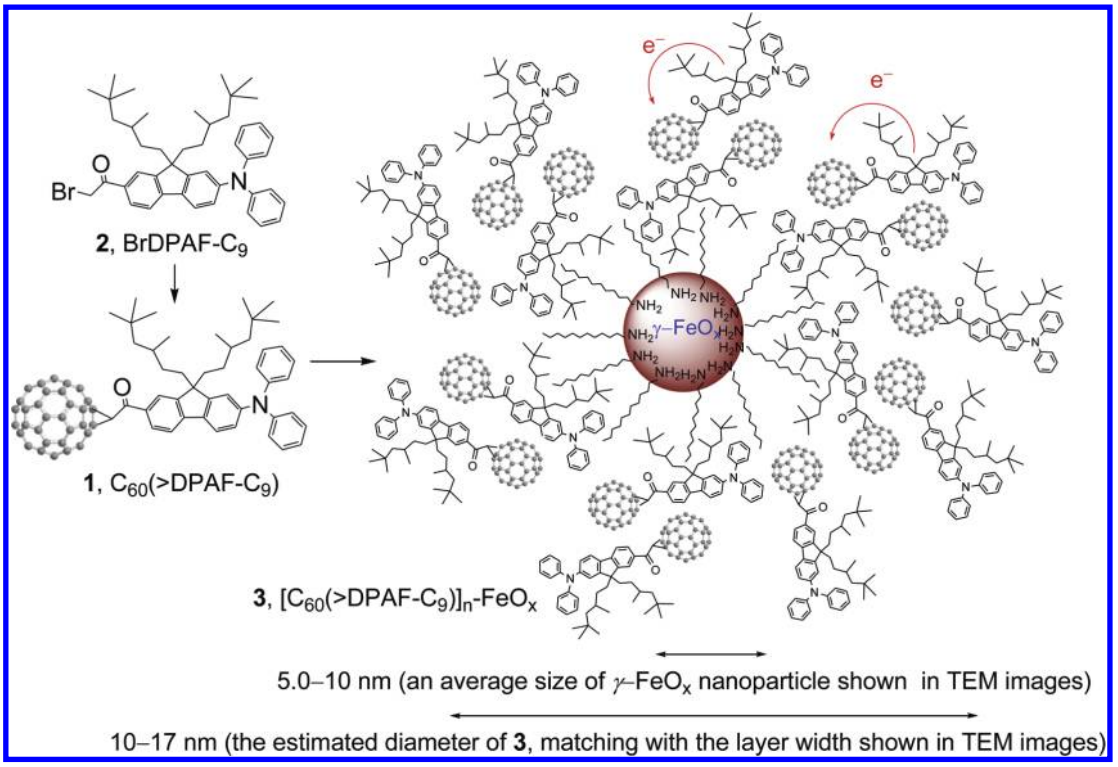

Figure 1. The key step in the synthesis of C_{60}(>DPAF-C_9) **1** and the schematic presentation of C_{60}(>DPAF-C_9)-encapsulated-FeO_x nanoparticles based on the average layer width and the diameter size observed in TEM micrographs (Figure 3).

1 (Figure 1), as a well-defined, covalently periconjugated acceptor–donor nanostructure, in a form of nanocomposite with magnetic γ-FeO_x aiming at the incorporation of delocalized π-electrons and spin-polarized d-electrons in one material system. Our experimental studies indicated that such a combination of π- and d-electrons is capable of generating simultaneously both density- and mobility-based MC, indicating the coexistence of excited-state effects and intercharge spin–spin interactions for the development of magneto-electronic properties using nanocomposites as the model. Observed events suggested the possibility of the MC modulation by the integration of intramolecularly charge-polarizable semiconducting C_{60}-diphenylaminofluorene monoadducts and magnetic oxide nanoparticles into one nanostructure system. To maximize the efficiency of interfacial molecular interactions, we calculated the quantity of **1** sufficient only to form either a monolayer or a bilayer encapsulation on the surface of oxide nanoparticles.

2. EXPERIMENTAL SECTION

The [60]fullerenyl nanostructure **1** was designed by incorporating a highly photoresponsive dialkyldiphenylaminofluorene (DPAF-C_n) donor chromophore subunit as an electromagnetic wave absorptive antenna in the visible range to facilitate the facile intramolecular electron transfer from this moiety to the electron-accepting C_{60} cage moiety at the excited state. The electron-transfer efficiency was optimized by attaching the DPAF-C_n unit at the close vicinity of a C_{60} cage in a contact distance of roughly <3.0 Å to fullerenyl π-electrons. This distance was verified by the X-ray single-crystal structural analysis of a closely related derivative C_{60}(>DPAF-C_2)[28] different from **1** only by the chain length of alkyl groups bound on DPAF. It is also coupled with a cyclopropanyl keto-linker to enable the keto–enol isomerization mechanism within the nanostructure **1** for enhancing ultrafast electron-transfer rate between the donor and acceptor subunits. The synthesis of C_{60}(>DPAF-C_9) was carried out by the cyclopropanation reaction of 7-bromoacetyl-9,9-di(3,5,5-trimethylhexyl)-2-diphenylaminofluorene **2** (BrDPAF-C_9), as a key precursor intermediate, with C_{60} in the presence of 1,8-diazabicyclo[5.4.0]undec-7-ene (DBU) at ambient temperature.[29,30] As the variation of preparative multistep synthetic conditions is possible, the purity of C_{60}(>DPAF-C_9) monoadduct applied was substantiated by both ^{1}H and ^{13}C NMR spectra (Supporting Information). The lowest unoccupied orbital (LUMO) of C_{60}(>DPAF-C_n), located at the electron-accepting C_{60} cage moiety, was found to be 1.73 eV above the highest occupied molecular orbital (HOMO), localized on the electron-donating DPAF-C_n moiety.[31] Excitation of **1** leads to singlet excited $^1C_{60}$*(>DPAF-C_n) state, followed by the charge-separated $C_{60}^{-\bullet}$(>DPAF$^{+\bullet}$-C_n) state through the intramolecular charge-transfer process (see the Supporting Information).

Synthesis of magnetic γ-FeO_x ($1.0 < x < 1.5$) nanoparticles was carried out by modifications of the literature procedures.[32,33] In a typical reaction, a mixture of $FeCl_3 \cdot 6H_2O$ (2.70 g, 0.010 mol), $FeCl_2 \cdot 4H_2O$ (1.98 g, 0.010 mol), sodium acetate (4.92 g, 0.060 mol, as a hydrolyzing agent), H_2O (4.0 mL), and *n*-octylamine (7.3 mL, as a capping agent) in 1,2-propanediol (66 mL) was prepared and stirred under reflux at 150 °C for a period of 5.0 h. It was followed by precipitation upon the addition of 2-propanol to afford the product in a nearly quantitative yield. Sufficient binding of *n*-octylamine, even though as a weak capping agent, on the surface of iron oxide nanoparticles modified the surface compatibility to organic substances and rendered their moderate solubility in organic solvents, such as toluene and chloroform. Therefore, encapsulation of γ-FeO_x nanoparticles by C_{60}(>DPAF-C_9) became possible and was carried out by dissolving the oxide particle (100 mg) in toluene with the aid of a small quantity of *n*-octylamine, followed by the addition of **1** (100 mg) and subsequent ultrasonication for a period of 30 min. After removal of toluene, encapsulated magnetic nanoparticles were washed repeatedly with 2-propanol and ether, followed by drying in a vacuum. Interestingly, the procedure resulted in a significant increase of the γ-FeO_x solubility in both toluene and $CHCl_3$, given the implication of successful encapsulation by C_{60}(>DPAF-C_9) with the most soluble structural moiety of 3,5,5-trimethylhexyl groups likely located at the outer-layer region of the composite particle **3** for interface with the

dx.doi.org/10.1021/ja210812u | J. Am. Chem. Soc. 2012, 134, 3549–3554

solvent, as shown in Figure 1. The atomic ratio of Fe^{2+} and Fe^{3+} applied in the preparation of magnetic oxide composites was tuned to enable the spin-exchange interactions[34] and intervalence charge transfer between irons in these two oxidation states. It will also allow the potential electron reduction of C_{60}(>DPAF-C_9) by the process of oxidative $Fe^{2+} \rightarrow Fe^{3+}$ conversion, resulting in an increase of Fe^{n+} component in a higher spin-state and the corresponding fullerene derivatives in a partially negative-charged state. Clearly, C_{60}(>DPAF-C_n) and γ-FeO_x are accountable for semiconducting and magnetic properties, respectively, in the designed fullerene nanoparticles. The DPAF-C_n donor moiety is then used to facilitate the charge transfer between itself and the fullerene cage for coupling π and d electrons under the magnetic field governed by γ-FeO_x.

Infrared spectra of γ-FeO_x (Figure 2a) and C_{60}(>DPAF-C_9) (Figure 2b) were applied as the comparison reference for the characterization

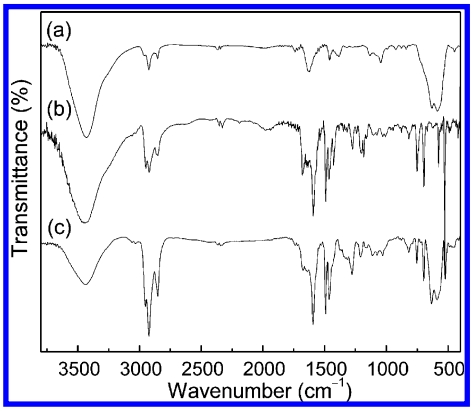

Figure 2. FT-IR spectra of (a) γ-FeO_x, (b) C_{60}(>DPAF-C_9), and C_{60}(>DPAF-C_9)-encapsulated magnetic γ-FeO_x nanoparticles.

of nanocomposite **3**. Detection of close superimposition of Figure 2a and b into the spectrum of C_{60}(>DPAF-C_9)-encapsulated γ-FeO_x (Figure 2c) revealed a roughly comparable quantity of γ-FeO_x and C_{60}(>DPAF-C_9) in **3**, showing the characteristic strong oxide bands at 584 and 632 cm^{-1} with sharp fullerenyl monoadduct bands at 752, 697, 576, and 526 cm^{-1} and a carbonyl stretching absorption peak centered at 1678 cm^{-1} consistent with those of the parent moieties.

The PMMA [poly(methyl methacrylate)] composite of **3** was prepared by a CH_2Cl_2 solution of C_{60}(>DPAF-C_9)-encapsulated γ-FeO_x in a concentration of 1.0×10^{-3} M under sonication, followed by casting it into a thin film for the magnetocurrent measurements. A portion of this solution was further diluted to solutions with concentrations of 1.0×10^{-4} and 1.0×10^{-5} M for subsequent transmission electron microscopy (TEM) measurements. As a result, several TEM micrographs displayed in Figure 3 showed many regular hard nanospheres in a size ranging from 5.0 to 10 nm in diameter (Figure 3a and b), encircled by an outer layer of C_{60}(>DPAF-C_9) in a thickness of ca. 2.0–3.0 nm, as shown in Figure 3b. This layer thickness matches well with the estimated partial bilayer molecular width of C_{60}(>DPAF-C_9). In addition, apparently visible contrast edges of fullerenes in a round sharp, as shown in the inset image of Figure 3b, being separated from the hard-sphere nanoparticle region led us to propose that C_{60} cages may not be located at the coating position in direct contact with the surface of γ-FeO_x nanoparticles.

The observation is reasonable by the fact that the *n*-octylamine-capping of oxide particles should favor its alkyl–alkyl interactions with the 3,5,5-trimethylhexyl moieties of **1** and thus directs the orientation of C_{60}(>DPAF-C_9) in **3** into a partial bilayer configuration to maximize also the C_{60}–C_{60} cage interactions, as depicted in Figure 1. In the case of Figure 3c, strong hydrophobic–hydrophobic interaction forces among C_{60} cages in the encapsulation layer seem to stabilize coated γ-FeO_x nanospheres, showing no clear evidence of disintegration of **1** from **3** during the addition of PMMA, as the thin film matrix. In fact, high incompatibility or immiscibility between C_{60} cages and PMMA should force C_{60}(>DPAF-C_9) molecules to retain at the surface of oxide nanoparticles and assists the structural stability of **3**.

MC measurements were performed by recording the electrical current as a function of applied magnetic field at a constant voltage (with the initial current at the level of 20 mA/cm^2) with different temperatures using thin-film semiconductor devices in this study. A typical device was fabricated with ITO (indium–tin–oxide) and Al (aluminum) electrodes to sandwich an active thin film with the ITO/fullerene composite/Al architecture. Specifically, [60]fullerenyl monoadduct **1**-encapsulated magnetic oxide nanoparticles **3** were mixed with PMMA by a variable weight ratio in chloroform solution. The solution was then spin-casted to form thin films with the thickness of 80 nm on precleaned ITO glass substrates. Subsequently, an Al electrode was deposited with the thickness of 50 nm on the surface of composite thin film via the thermal evaporation technique under the vacuum of 2.0×10^{-6} Torr. The amplitude of measured MC was defined as $MC = ((I_B - I_0)/I_0) \times 100\%$, where I_B and I_0 are the electrical currents with and without magnetic field, respectively.

3. RESULTS AND DISCUSSION

Magnetic Hysteresis and Magnetocurrent. Two thin-film devices derived from either C_{60}(>DPAF-C_9) **1**-encapsulated γ-FeO_x (1:1, w/w) in PMMA matrix (magnetic fullerene composite **A**) or C_{60}(>DPAF-C_9) in PMMA matrix (nonmagnetic fullerene composite **B**) were applied for the MC measurements. The latter sample is oxide-free and nonmagnetic for the property comparison with the former magnetic one. As a result, the MC of both magnetic and nonmagnetic fullerene composites at 77 K were depicted in Figure 4a. It is interesting to note that the MC from the magnetic composite **A** can be reconvoluted into two curve profile components each with a different slope, as the first segment showed a gradual increase from 0 to 30 mT and the second segment turned to a more dramatic increase from 30 to 300 mT. A distinguishably different behavior on the MC profile of the nonmagnetic composite **B** was detected showing a gradual increase from 0 to 50 mT initially, followed by a saturation of MC from 50 to 300 mT. This represents as a typical curve shape for many organic semiconductors.[35,36] Two MC profile segments of the magnetic fullerene composite **A** material can be interpreted as follows: the first part arising from the density channel via magnetic field-dependent populations of singlet and triplet excited states and the second part resulting from the mobility channel via intercharge spin interactions. It is observable in Figure 4b that C_{60}(>DPAF-C_9)-encapsulated γ-FeO_x **3** materials exhibit magnetic hysteresis curves at different temperatures of 90 and 300 K. These hysteresis curves indicated that the critical temperature of the encapsulated magnetic nanoparticle **3** is higher than 300 K with the saturation magnetization at a value of 5.1 μ_B per formula unit. Theoretically, the expected saturation values of Fe^{3+} oxide with a spin state $S = 5/2$ is 5.0 μB per formula unit. Therefore, the measured experimental saturation value of **3** matches well with the high-spin Fe^{3+} as the main oxide composition, even though a mixture of Fe^{3+} and Fe^{2+} precursor molecules in a comparable quantity was applied in the preparation of **3**. Coercive field of less than 1 mT measured at 300 K is most likely due to the remnant field of superconducting magnet used for the measurement.

Figure 5a showed the normalized curves of both hysteresis and MC data for the magnetic compiste **A** (C_{60}(>DPAF-C_9) **1**-encapsulated γ-FeO_x (1:1, w/w) in PMMA matrix) at low temperatures to further understand the MC contributions from semiconducting and magnetic structures. It should be pointed out that the former curve profile has a different shape as

dx.doi.org/10.1021/ja210812u | J. Am. Chem. Soc. 2012, 134, 3549–3554

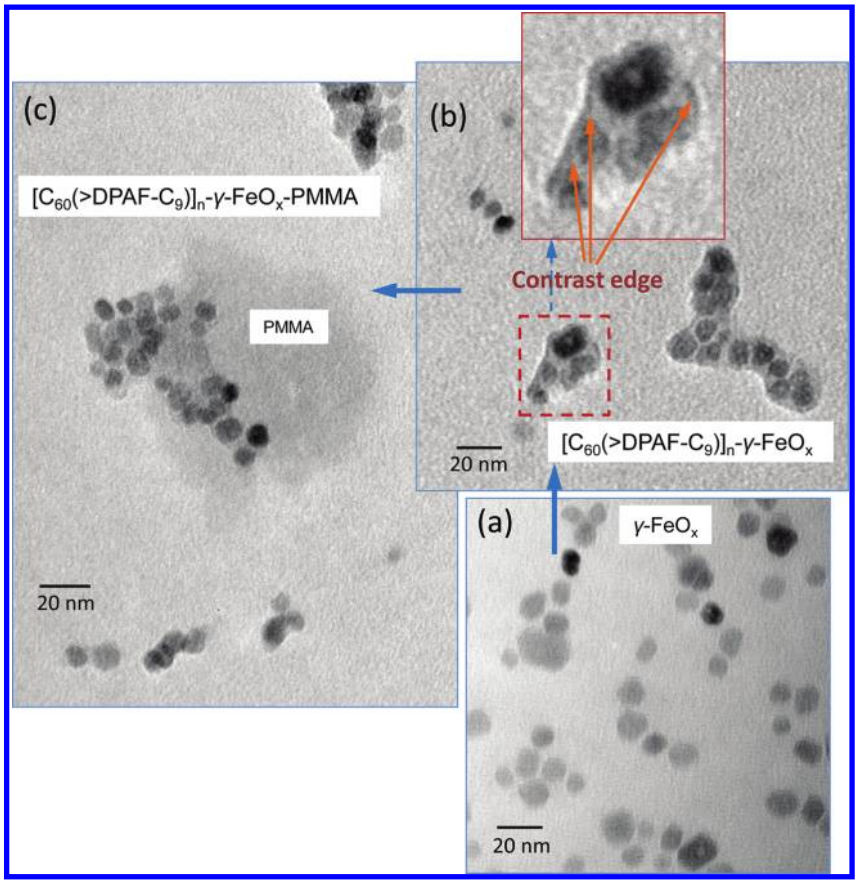

Figure 3. TEM micrographs of (a) γ-FeO_x nanoparticles, (b) C_{60}(>DPAF-C_9) **1**-encapsulated γ-FeO_x nanoparticles showing a nearly mono- to bilayered molecular width of **1**, and (c) impregnated (b) in PMMA matrix.

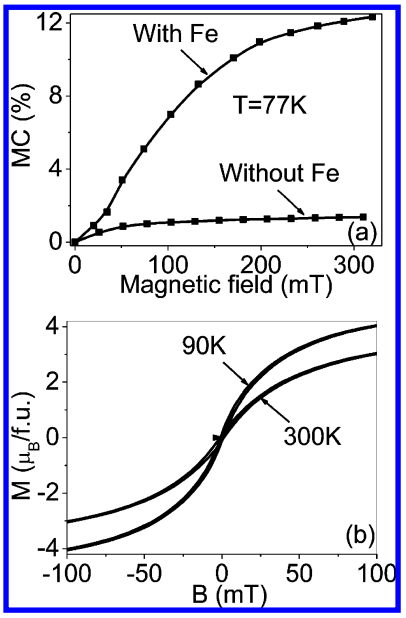

Figure 4. (a) Magnetocurrents for Fe-free and Fe-containing C_{60} composite devices at 77 K. (b) *M* versus *H* hysteresis loops for Fe-containing C_{60} composite recorded at 90 and 300 K, respectively.

compared to that of the latter one. This implied the MC occurring in the magnetic fullerene composite **A**-based thin film not only arising from intercharge spin−spin interactions, via magnetism, but rather with an additional involvement of excited-state populations. Accordingly, the data support our proposed magnetoelectronic mechanism that the MC of the magnetic composite **A** consists of both the density-based component through the population of excited states, which originated from the charge-polarizable fullerenyl chromophore structure, and the mobility-based component facilitated by intercharge spin interactions through magnetism existing in the magnetic oxide structure of γ-FeO_x.

Theroretical Analysis and Experimental Data Fitting. To further understand the differentiation and contribution of mobility-based MC from magnetic structure and density-based MC from semiconducting structure, the curve fitting was performed by combining a typical MC from organic semiconducting materials and the magnetization from inorganic magnetic materials. Accordingly, the MC component from an organic semiconducting structure can be given by:[35,36]

$$MC(B) = P_1 h(B) = P_1 \frac{B^2}{(|B| + B_0)^2} \quad (1)$$

where P_1 is the MC coefficient of the semiconducting structure, B is the magnetic field, and B_0 is the internal magnetic interaction via either hyperfine interaction or spin−orbital coupling. By fitting the MC from the nonmagnetic C_{60} nanoparticles versus B, we determined the internal magnetic interaction parameter B_0 = 17.16 mT.

In the case of the MC in the magnetic structure, the magnetic hysteresis curve can be used to reflect the magnetization. Furthermore, the spin scattering-based MC was found to be proportional to the square of magnetization.[37,38] Therefore, the mobility-based MC from intercharge spin interactions through

dx.doi.org/10.1021/ja210812u | J. Am. Chem. Soc. 2012, 134, 3549−3554

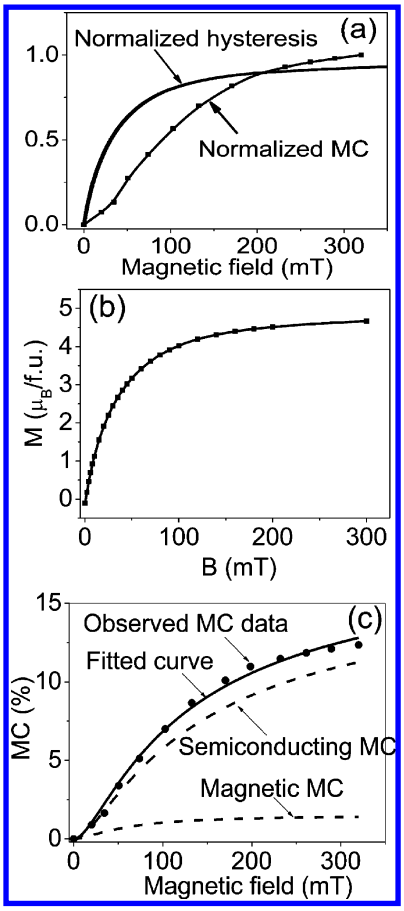

Figure 5. (a) Normalized hysteresis curve at 90 K and normalized MC curve at 77 K for magnetic C_{60} derivative, (b) curve fitting (−) and experimental data (■) for hysteresis of magnetic C_{60} derivative at 90 K, and (c) curve fitting (−) and experimental data (●) for MC from magnetic C_{60} composite **A**. Two dashed lines represent two MC components, from curve fitting, for semiconducting and magnetic structures in C_{60}(>DPAF-C_9) **1**-encapsulated γ-FeO_x particles.

magnetism can be written as $MC(B) = P_2m^2(B)$, where P_2 is the mobility enhancement coefficient caused by magnetic dipoles, and $m(B)$ is the magnetization in the field increasing direction. As a result, the combined MC is given by:

$$MC(B) = \frac{I_B - I_0}{I_0} = \frac{I_0*[1 + P_1h(B)]*[1 + P_2m^2(B)] - I_0}{I_0} = P_1h(B) + P_2m^2(B) + P_1P_2h(B)m^2(B) \quad (2)$$

where $h(B) = (B^2/(|B| + B_0)^2)$ and $m(B) = A_1 \exp(-B/t_1) + A_2 \exp(-B/t_2) + A_3 \exp(-B/t_3) + y_0$.

The curve fitting of the hysteresis data (Figure 5b) at 90 K yielded $A_1 = -3.2979$, $t_1 = 44.45663$, $A_2 = -0.80581$, $t_2 = 241.63283$, $A_3 = -0.91938$, $t_3 = 11.09026$, and $y_0 = 4.90316$. On the basis of the combined MC values given by eq 2, we can fit the experimental MC data, obtained from the magnetic C_{60} composite **A** at 77 K, with $P_1 = 0.16795$, $P_2 = 0.00064$, as shown in Figure 5c. Results of these curve fittings agreed well with the condition that both density- and mobility-based components applied.

As the temperature increases to 300 K, the MC from magnetic composite **A**, C_{60}(>DPAF-C_9)-encapsulated oxide **3**, shows a one-component curve profile as compared to the two-component curve profile at 77 K (Figure 6a). Therefore, the

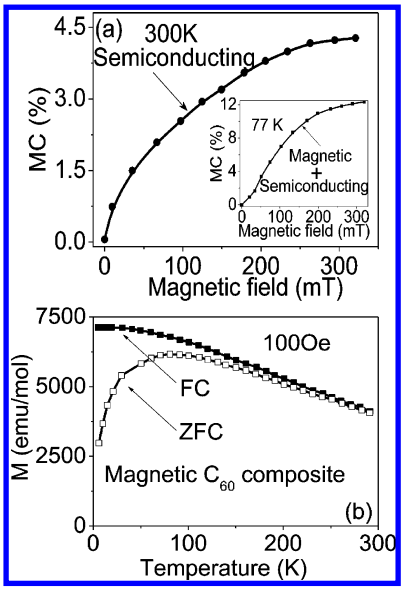

Figure 6. (a) Magnetocurrent for Fe-containing C_{60} composite with ITO and Al electrodes at 300 K. The C_{60} derivatives are dispersed into PMMA matrix with the weight ratio of 2:4. The inset shows the MC curve for Fe-containing C_{60} composite device at 77 K as a comparison. (b) Variation of zero field cooled (ZFC) and field cooled (FC) magnetization with temperature measured at an applied magnetic field of 100 Oe for Fe-containing C_{60} composite.

magnetic component of MC from magnetic composite **A** becomes negligible at 300 K. This means that the contribution from the density-based MC is a dominant component in the thin film of magnetic composite **A** at room temperature. This observation allowed us to correlate the detected MC dominantly to the contribution of the C_{60}(>DPAF-C_9) moiety of the magnetic composite **3** at 300 K, whereas at 77 K the mobility-based MC component was contributed from the magnetic γ-FeO_x moiety. A large reduction of the magnetic component at high temperature can be correlated to the decrease of magnetization upon the increase of temperature to 300 K on the same analogue composite, as shown in Figure 6b.

4. CONCLUSIONS

We demonstrated that incorporating a delocalized π-electron system in a closely bound acceptor−donor analogue chromophore, involving highly charge-polarizable C_{60}(>DPAF-C_9) nanostructure **1**, and spin-polarized d-electrons in a form of encapsulated γ-FeO_x nanoparticles can form a coexisted semiconducting and magnetic system. Because of the facile intramolecular electron transfer from the DPAF-C_9 donor moiety to the C_{60} acceptor cage of **1**,[39,40] the C_{60}(>DPAF-C_9)-encapsulated magnetic γ-FeO_x nanoparticle composite exhibited an interesting MC behavior that was elucidated to consist of the mobility-based MC through the magnetism of spin-polarized d-electrons, the density-based MC through excited states of delocalized π-electrons, and the mobility-density coupled MC through the coupling between π- and d-electrons. Interestingly, by changing the temperature, it led to a modification in the weight ratio between these two MC

dx.doi.org/10.1021/ja210812u | J. Am. Chem. Soc. 2012, 134, 3549−3554

components. Specifically, at 77 K, the measured MC contains a contribution from the magnetism of spin-polarized d-electrons, the mobility-based MC. At the higher temperature region up to 300 K, the measured MC was found to be correlated to a major contribution from the spin-dependent population at excited states of delocalized π-electrons, the density-based MC. These results may provide a clear implication of the magnetocurrent modulation by the integration of semiconducting organics and magnetic inorganic structures into one nanocomposite material via the encapsulation technique to create a largely enhanced interfacial surface area with efficient charge and spin interactions for magneto-electronics.

■ ASSOCIATED CONTENT

Supporting Information

Spectroscopic characterization of chromatographically purified C_{60}(>DPAF-C_9) nanostructure, proof of a monoadduct structure of the C_{60}(>DPAF-C_9) sample, energy diagram of materials, and the current−voltage characteristics for magnetic and nonmagnetic C_{60} composite devices. This material is available free of charge via the Internet at http://pubs.acs.org.

■ AUTHOR INFORMATION

Corresponding Author

bhu@utk.edu; long_chiang@uml.edu

Notes

The authors declare no competing financial interest.

■ ACKNOWLEDGMENTS

L.Y. and B.H. would like to acknowledge financial support from the Air Force Office of Scientific Research (AFOSR) under grant number FA9550-11-1-0082 and from the NSF under grant number ECCS-0644945. M.W. and L.Y.C. are thankful for the financial support of AFOSR under grant number FA9550-09-1-0380 and the Air Force Research Laboratory (AFRL) under contract number FA8650-09-D-5037-0006.

■ REFERENCES

(1) Hanasaki, N.; Tajima, H.; Matsuda, M.; Naito, T.; Inabe, T. *Phys. Rev. B* **2000**, *62*, 5839.
(2) Prigodin, V.; Raju, N.; Pokhodnya, K.; Miller, J.; Epstein, A. *Adv. Mater.* **2002**, *14*, 1230.
(3) Miyazaki, A.; Enomoto, K.; Okabe, K.; Yamazaki, H.; Nishijo, J.; Enoki, T.; Ogura, E.; Ugawa, K.; Kuwatani, Y.; Iyoda, M. *J. Solid State Chem.* **2002**, *168*, 547.
(4) Raju, N. P.; Savrin, T.; Prigodin, V. N.; Pokhodnya, K. I.; Miller, J. S.; Epstein, A. J. *J. Appl. Phys.* **2003**, *93*, 6799.
(5) Nishijo, J.; Miyazaki, A.; Enoki, T.; Watanabe, R.; Kuwatani, Y.; Iyoda, M. *Inorg. Chem.* **2005**, *44*, 2493.
(6) Matsushita, M. M.; Kawakami, H.; Sugawara, T.; Ogata, M. *Phys. Rev. B* **2008**, *77*, 195208.
(7) Komatsu, H.; Mogi, R.; Matsushita, M. M.; Miyagi, T.; Kawada, Y.; Sugawara, T. *Polyhedron* **2009**, *28*, 1996.
(8) Ishikawa, M.; Asari, T.; Matsuda, M.; Tajima, H.; Hanasaki, N.; Naito, T.; Inabe, T. *J. Mater. Chem.* **2010**, *20*, 4432.
(9) Sugawara, T.; Komatsu, H.; Suzuki, K. *Chem. Soc. Rev.* **2011**, *40*, 3105.
(10) Kalinowski, J.; Cocchi, M.; Virgili, D.; Di Marco, P.; Fattori, V. *Chem. Phys. Lett.* **2003**, *380*, 710.
(11) Prigodin, V. N.; Bergeson, J. D.; Lincoln, D. M.; Epstein, A. J. *Synth. Met.* **2006**, *156*, 757.
(12) Desai, P.; Shakya, P.; Kreouzis, T.; Gillin, W. P. *J. Appl. Phys.* **2007**, *102*, 073710.
(13) Majumdar, S.; Majumdar, H. S.; Aarnio, H.; Osterbacka, R. *Phys. Status Solidi RRL* **2009**, *3*, 242.
(14) Francis, T. L.; Mermer, Ö.; Veeraraghavan, G.; Wohlgenannt, M. *New J. Phys.* **2004**, *6*, 185.
(15) Mermer, Ö.; Veeraraghavan, G.; Francis, T. L.; Wohlgenannt, M. *Solid State Commun.* **2005**, *134*, 631.
(16) Bobbert, P. A.; Nguyen, T. D.; van Oost, F. W. A.; Koopmans, B.; Wohlgenannt, M. *Phys. Rev. Lett.* **2007**, *99*, 216801.
(17) Wagemans, W.; Bloom, F. L.; Bobbert, P. A.; Wohlgenannt, M.; Koopmans, B. *J. Appl. Phys.* **2008**, *103*, 07F303.
(18) Ikegami, T.; Kawayama, I.; Tonouchi, M.; Nakao, S.; Yamashita, Y.; Tada, H. *Appl. Phys. Lett.* **2008**, *92*, 153304.
(19) Hu, B.; Wu, Y. *Nat. Mater.* **2007**, *6*, 985.
(20) Bergeson, J. D.; Prigodin, V. N.; Lincoln, D. M.; Epstein, A. J. *Phys. Rev. Lett.* **2008**, *100*, 067201.
(21) Hu, B.; Yan, L.; Shao, M. *Adv. Mater.* **2009**, *21*, 1500.
(22) Garditz, C.; Muckl, A. G.; Colle, M. *J. Appl. Phys.* **2005**, *98*, 104507.
(23) Yusoff, A. R. B. M.; da Silva, W. J.; Serbena, J. P. M.; Meruvia, M. S.; Hummelgen, I. A. *Appl. Phys. Lett.* **2009**, *94*, 253305.
(24) Song, J. Y.; Stingelin, N.; Drew, A. J.; Kreouzis, T.; Gillin, W. P. *Phys. Rev. B* **2010**, *82*, 085205.
(25) Li, F.; Xin, L.; Liu, S.; Hu, B. *Appl. Phys. Lett.* **2010**, *97*, 073301.
(26) Baibich, M. N.; Broto, J. M.; Fert, A.; Van Dau, F. N.; Petroff, F.; Etienne, P.; Creuzet, G.; Friederich, A.; Chazelas, J. *Phys. Rev. Lett.* **1988**, *61*, 2472.
(27) von Helmolt, R.; Wecker, J.; Holzapfel, B.; Schultz, L.; Samwer, K. *Phys. Rev. Lett.* **1993**, *71*, 2331.
(28) Padmawar, P. A.; Rogers, J. E.; He, G. S.; Chiang, L. Y.; Tan, L.-S.; Canteenwala, T.; Zheng, Q.; Slagle, J. E.; McLean, D. G.; Fleitz, P. A.; Prasad, P. N. *Chem. Mater.* **2006**, *18*, 4065.
(29) Padmawar, P. A.; Canteenwala, T.; Verma, S.; Tan, L.-S.; Chiang, L. Y. *J. Mater. Chem.* **2006**, *16*, 1366.
(30) Jeon, S.; So, G.; Anandakathir, R.; Canteenwala, T.; Tan, L. S.; Pritzker, K.; Chiang, L. Y. *J. Macromol. Sci., Part A: Pure Appl. Chem.* **2008**, *45*, 918.
(31) Luo, H.; Fujitsuka, M.; Araki, Y.; Ito, O.; Padmawar, P.; Chiang, L. Y. *J. Phys. Chem. B* **2003**, *107*, 9312.
(32) Rajamathi, M.; Ghosh, M.; Seshadri, R. *Chem. Commun.* **2002**, 1152.
(33) Mikami, R.; Taguchi, M.; Yamada, K.; Suzuki, K.; Sato, O.; Einaga, Y. *Angew. Chem.* **2004**, *116*, 6261.
(34) Awaga, K.; Okuno, T.; Yamaguchi, A.; Hasegawa, M.; Inabe, T.; Maruyama, Y.; Wada, N. *Phys. Rev. B* **1994**, *49*, 3975.
(35) Mermer, Ö.; Veeraraghavan, G.; Francis, T. L.; Sheng, Y.; Nguyen, D. T.; Wohlgenannt, M.; Köhler, A.; Al-Suti, M. K.; Khan, M. S. *Phys. Rev. B* **2005**, *72*, 205202.
(36) Sheng, Y.; Nguyen, T. D.; Veeraraghavan, G.; Mermer, O.; Wohlgenannt, M.; Qiu, S.; Scherf, U. *Phys. Rev. B* **2006**, *74*, 045213.
(37) Yosida, K. *Phys. Rev.* **1957**, *107*, 396.
(38) Hedgcock, F. T.; Muir, W. B.; Raudorf, T. W.; Szmidt, R. *Phys. Rev. Lett.* **1968**, *20*, 457.
(39) Luo, H.; Fujitsuka, M.; Araki, Y.; Ito, O.; Padmawar, P.; Chiang, L. Y. *J. Phys. Chem. B* **2003**, *107*, 9312.
(40) El-Khouly, M. E.; Anandakathir, R.; Ito, O.; Chiang, L. Y. *J. Phys. Chem. A* **2007**, *111*, 6938.